

University of Groningen

Comparison of Improved Unidirectional Dual Velocity-Encoding MRI Methods

Franco, Pamela; Ma, Liliana; Schnell, Susanne; Carrillo, Hugo; Montalba, Cristian; Markl, Michael; Bertoglio, Cristóbal; Uribe, Sergio

Published in:
Journal of Magnetic Resonance Imaging

DOI:
[10.1002/jmri.28305](https://doi.org/10.1002/jmri.28305)

IMPORTANT NOTE: You are advised to consult the publisher's version (publisher's PDF) if you wish to cite from it. Please check the document version below.

Document Version
Publisher's PDF, also known as Version of record

Publication date:
2023

[Link to publication in University of Groningen/UMCG research database](#)

Citation for published version (APA):

Franco, P., Ma, L., Schnell, S., Carrillo, H., Montalba, C., Markl, M., Bertoglio, C., & Uribe, S. (2023). Comparison of Improved Unidirectional Dual Velocity-Encoding MRI Methods. *Journal of Magnetic Resonance Imaging*, 57(3), 763-773. <https://doi.org/10.1002/jmri.28305>

Copyright

Other than for strictly personal use, it is not permitted to download or to forward/distribute the text or part of it without the consent of the author(s) and/or copyright holder(s), unless the work is under an open content license (like Creative Commons).




The publication may also be distributed here under the terms of Article 25fa of the Dutch Copyright Act, indicated by the "Taverne" license. More information can be found on the University of Groningen website: <https://www.rug.nl/library/open-access/self-archiving-pure/taverne-amendment>.

Take-down policy

If you believe that this document breaches copyright please contact us providing details, and we will remove access to the work immediately and investigate your claim.

Downloaded from the University of Groningen/UMCG research database (Pure): <http://www.rug.nl/research/portal>. For technical reasons the number of authors shown on this cover page is limited to 10 maximum.

Comparison of Improved Unidirectional Dual Velocity-Encoding MRI Methods

Pamela Franco, MSc,^{1,2,3,4}  Liliana Ma, PhD,^{5,6}  Susanne Schnell, PhD,⁷ 
 Hugo Carrillo, PhD,^{8,9} Cristian Montalba, BSc,^{1,3,10} Michael Markl, PhD,^{5,6}
 Cristóbal Bertoglio, PhD,¹¹ and Sergio Uribe, PhD^{1,3,4,10*}

Background: In phase-contrast (PC) MRI, several dual velocity encoding methods have been proposed to robustly increase velocity-to-noise ratio (VNR), including a standard dual-VENC (SDV), an optimal dual-VENC (ODV), and bi- and tri-conditional methods.

Purpose: To develop a correction method for the ODV approach and to perform a comparison between methods.

Study Type: Case-control study.

Population: Twenty-six volunteers.

Field Strength/Sequence: 1.5 T phase-contrast MRI with VENCs of 50, 75, and 150 cm/second.

Assessment: Since we acquired single-VENC protocols, we used the background phase from high-VENC (VENC_H) to reconstruct the low-VENC (VENC_L) phase. We implemented and compared the unwrapping methods for different noise levels and also developed a correction of the ODV method.

Statistical Tests: Shapiro-Wilk's normality test, two-way analysis of variance with homogeneity of variances was performed using Levene's test, and the significance level was adjusted by Tukey's multiple post hoc analysis with Bonferroni ($P < 0.05$).

Results: Statistical analysis revealed no extreme outliers, normally distributed residuals, and homogeneous variances. We found statistically significant interaction between noise levels and the unwrapping methods. This implies that the number of non-unwrapped pixels increased with the noise level. We found that for $\beta = \text{VENC}_L/\text{VENC}_H = 1/2$, unwrapping methods were more robust to noise. The post hoc test showed a significant difference between the ODV corrected and the other methods, offering the best results regarding the number of unwrapped pixels.

Data Conclusions: All methods performed similarly without noise, but the ODV corrected method was more robust to noise at the price of a higher computational time.

Level of Evidence: 4

Technical Efficacy Stage: 1

J. MAGN. RESON. IMAGING 2023;57:763-773.

Phase-contrast (PC) MRI enables the quantification of velocities by subtracting two measured phases of the complex transverse magnetization.¹ This method was extended to 4D-flow MRI, which was applied in several studies for the quantitative analysis of cardiovascular diseases.²⁻⁸ However, the applications of 2D PC-MRI and 4D flow may be limited

by the low velocity-to-noise ratio (VNR) of the images. The VNR is mainly managed by setting the velocity-encoding sensitivity (VENC). VENC is inversely proportional to VNR in the final measured velocity map. However, if VENC is lower than the maximum velocity, it leads to phase wrapping in the velocity data.⁹ Furthermore, even for VENC values slightly

View this article online at wileyonlinelibrary.com. DOI: 10.1002/jmri.28305

Received Apr 12, 2022, Accepted for publication May 31, 2022.

*Address reprint requests to: S.U., Department of Radiology and Biomedical Imaging Center, School of Medicine, Pontificia Universidad Católica de Chile, Marcoleta 367, Santiago, Chile. E-mail: suribe@uc.cl

Cristóbal Bertoglio and Sergio Uribe are joint last authors.

From the ¹Biomedical Imaging Center, School of Engineering, Pontificia Universidad Católica de Chile, Santiago, Chile; ²Electrical Engineering Department, School of Engineering, Pontificia Universidad Católica de Chile, Santiago, Chile; ³Millennium Nucleus for Cardiovascular Magnetic Resonance, Santiago, Chile;

⁴Instituto Milenio Intelligent Healthcare Engineering, Santiago, Chile; ⁵Department of Radiology, Feinberg School of Medicine, Northwestern University, Chicago, Illinois, USA; ⁶Department of Biomedical Engineering, McCormick School of Engineering, Northwestern University, Evanston, Illinois, USA; ⁷Institut für Physik, Universität Greifswald, Greifswald, Germany; ⁸Center for Mathematical Modeling, Universidad de Chile, Santiago, Chile; ⁹Inria Chile Research Center, Santiago, Chile; ¹⁰Radiology Department, School of Medicine, Pontificia Universidad Católica de Chile, Santiago, Chile; and ¹¹Bernoulli Institute, University of Groningen, Groningen, The Netherlands

Additional supporting information may be found in the online version of this article

larger than the true velocity, velocity aliasing may occur due to measurement noise.^{10–12}

Therefore, setting up the VENC is important to obtain velocity data with high VNR without wrapping artifacts. If the images have severe wrapping artifacts or low VNR, several images may need to be re-acquired with different VENCs, further increasing total scanning time.¹

In some cases, it is necessary to obtain quantitative information of low and high blood flow velocities simultaneously within the same field of view. For instance, velocities from veins and arteries can differ by orders of magnitude, even in normal subjects. Unwrapping methods are used as an additional post-processing step to be able to acquire data with as high as possible VNR and low as possible velocity sensitivity.¹³ In principle, phase unwrapping seems like a simple operation, which detects phase jumps and adds (or subtracts) the appropriate multiple of 2π to remove velocity wrapping. Nevertheless, the presence of noise, processing errors, undersampling, and spurious artifacts converts this problem into a cumbersome process, especially if the data experiences multiple wraps. To solve this issue, dual-VENC approaches have been proposed.

Lee et al first implemented dual-VENC 2D PC-MRI with through-plane velocity encoding that acquired three phases with different velocity encoding gradients, allowing reconstruction of two sets of velocity images corresponding to a high- and low-VENC. The low-VENC image was then unwrapped using the high-VENC.¹⁴ We call here this method standard dual-VENC (SDV). The result is a single dataset with the favorable VNR of the low-VENC scan but without velocity aliasing.

Furthermore, Schnell et al developed a dual-VENC 4D-flow MRI sequence using a shared reference scan followed by two successive interleaved high and low VENC acquisitions, which allowed the encoding of 3D blood flow velocities with a seven-point encoding scheme.¹⁵ In this context, a different dual-VENC reconstruction method consisting of the high VENC data to correct for aliasing in the low VENC data based on empirically defined thresholds. Recently, Ma et al proposed two improved ways to perform the dual-VENC reconstruction based on fixed thresholds using biconditional and triconditional statements.¹⁶

Carrillo et al reformulated the phase-contrast velocity as a least-squares estimator. The method was called optimal dual-VENC (ODV) and justified theoretically high/low VENC ratios such that the aliasing velocity can be minimized.¹⁷ The ODV formulation can be generalized to multiple-motion encoding in a straightforward manner, as it was done by Herthum et al,¹⁸ where it was also successfully applied to MR elastography in the brain.

In this study, we aimed to compare the SDV, ODV, bi-, and triconditional unwrapping methods under different noise conditions. In addition, we proposed a correction algorithm for the ODV method to improve the success of the methods, which is based on theoretical considerations.

Theory

Assumptions

We assume three measurements with gradients $G_0 = 0 < G_H < G_L$, this results in three measured phases φ_0 , φ_H , and φ_L . Two motion images with normal distribution can then be estimated that share the background phase, φ_0 , from the three-phase measurements:

$$u_H = \frac{\varphi_H - \varphi_0}{\pi} \text{VENC}_H, u_H \sim \mathcal{N}\left(\overline{u}_H, 2\sigma_\varphi^2 \text{VENC}_H^2\right)$$

$$u_L = \frac{\varphi_L - \varphi_0}{\pi} \text{VENC}_L, u_L \sim \mathcal{N}\left(\overline{u}_L, 2\sigma_\varphi^2 \text{VENC}_L^2\right) \quad (1)$$

u_H and u_L are related to velocities acquired with high- and low-VENCs, where $\text{VENC}_L = \beta \text{VENC}_H$, $0 < \beta < 1$, \overline{u}_H and \overline{u}_L are the mean velocity of the high- and low-VENCs, respectively, the value of σ_φ^2 depends on the SNR of the magnetization measurements, and the variance of u_H and u_L —after successful unwrapping—are respectively, $\text{Var}(u_H) = 2\sigma_\varphi^2 \text{VENC}_H^2$ and $\text{Var}(u_L) = 2\sigma_\varphi^2 \text{VENC}_L^2$. The four unwrapping methods that were investigated in this study are further described below.

Standard Dual-VENC Approach

Given two images with different VENC values, dual-VENC reconstructions aim to unwrap a set of velocity images acquired with a low VENC using an image acquired with a high VENC as follows:

$$k = \text{NI} \left(\frac{u_{\text{high}} - u_L}{2\text{VENC}_L} \right) u_{\text{SDV}} = u_L + 2\text{VENC}_L k \quad (2)$$

with NI the nearest integer operator and u_{high} computed as,

$$u_{\text{high}} = \begin{cases} u_i & i\text{VENC} > \text{VENC}_H \\ u_H & \text{otherwise} \end{cases} \quad (3)$$

where u_i is defined as,

$$u_i = \frac{\varphi_L - \varphi_H}{\pi} i\text{VENC} \quad (4)$$

The resulting third VENC depends on the change in first gradient moment between the low- and high-VENCs, is defined as,

$$i\text{VENC} = \frac{\text{VENC}_H \text{VENC}_L}{\text{VENC}_H - \text{VENC}_L} \quad (5)$$

We made a minor modification of the standard dual-VENC (SDV) reported Lee et al,¹⁴ in order to make a fair comparison with the other methods. We took full advantage of the VENCs used, in case $i\text{VENC} > \text{VENC}_H$, we used u_i

rather than u_H as the original SDV would have used, maintaining the effective VENC value. Note that $VENC_L < VENC_H \leq iVENC$.

Biconditional Approach

Following the logic of Dual-VENC methods proposed by Schnell et al,¹⁵ Ma et al¹⁶ used three sets of phase-contrast images (u_i, u_H, u_L) to identify wrapped voxels in the lowest VENC image.

First, a biconditional unwrapping method was proposed by an extension of Equation (2), where the aliased velocities fell into two categories:

$$\begin{aligned}
 VENC_L < u_L - u_i < 3VENC_L : u_{\text{biconditional}} &= u_L + 2VENC_L \\
 -3VENC_L < u_L - u_i < -VENC_L : u_{\text{biconditional}} &= u_L - 2VENC_L \\
 3VENC_L < u_L - u_i < 5VENC_L : u_{\text{biconditional}} &= u_L + 4VENC_L \\
 -5VENC_L < u_L - u_i < -3VENC_L : u_{\text{biconditional}} &= u_L - 4VENC_L
 \end{aligned}$$

and

$$\begin{aligned}
 VENC_H < u_H - u_i < 3VENC_H : u_{\text{biconditional}} &= u_L + 2VENC_L \\
 -3VENC_H < u_H - u_i < -VENC_H : u_{\text{biconditional}} &= u_L - 2VENC_L \\
 3VENC_H < u_H - u_i < 5VENC_H : u_{\text{biconditional}} &= u_L + 4VENC_L \\
 -5VENC_H < u_H - u_i < -3VENC_H : u_{\text{biconditional}} &= u_L - 4VENC_L
 \end{aligned} \tag{6}$$

Triconditional Approach

Also, in Ma et al,¹⁶ following the same strategy refers in the biconditional unwrapping method, the triconditional reconstruction algorithm also considered the relationship between the low- and high-VENC images, using the same two aliased velocity categories, with a new last condition. It brings the high- and low-VENCs into the same VENC domain and adds an additional constraint to prevent incorrect unwrapping of aliased voxels.

$$\begin{aligned}
 VENC_L < u_L - u_i < 3VENC_L : u_{\text{triconditional}} &= u_L + 2VENC_L \\
 -3VENC_L < u_L - u_i < -VENC_L : u_{\text{triconditional}} &= u_L - 2VENC_L \\
 3VENC_L < u_L - u_i < 5VENC_L : u_{\text{triconditional}} &= u_L + 4VENC_L \\
 -5VENC_L < u_L - u_i < -3VENC_L : u_{\text{triconditional}} &= u_L - 4VENC_L
 \end{aligned} \tag{7}$$

and

$$\begin{aligned}
 VENC_H < u_H - u_i < 3VENC_H : u_{\text{triconditional}} &= u_L + 2VENC_L \\
 -3VENC_H < u_H - u_i < -VENC_H : u_{\text{triconditional}} &= u_L - 2VENC_L \\
 3VENC_H < u_H - u_i < 5VENC_H : u_{\text{triconditional}} &= u_L + 4VENC_L \\
 -5VENC_H < u_H - u_i < -3VENC_H : u_{\text{triconditional}} &= u_L - 4VENC_L
 \end{aligned}$$

or

$$\begin{aligned}
 VENC_i < u_H - u_L < iVENC : u_{\text{triconditional}} &= u_L + 2VENC_L \\
 -3VENC_i < u_H - u_L < -iVENC : u_{\text{triconditional}} &= u_L - 2VENC_L \\
 3VENC_i < u_H - u_L < 5iVENC : u_{\text{triconditional}} &= u_L + 4VENC_L \\
 -5VENC_i < u_H - u_L < -3iVENC : u_{\text{triconditional}} &= u_L - 4VENC_L
 \end{aligned}$$

Optimal Dual-VENC Approach

Carrillo et al¹⁷ proposed the optimal dual-VENC (ODV) method. This method is based on the formulation of the dual-VENC problem as a least-squares sum function. The cost function has the form:

$$J_{\text{dual}}(u) = \sum_{j=1}^2 \left(1 - \cos\left(\frac{\pi}{VENC_j}(u_j - u)\right) \right) \tag{8}$$

In ODV, the unwrapped motion corresponds to the global minimum with the smallest magnitude, which we will denote u^* . Note that the periodicity of $J_{\text{dual}}(u)$ is the least common multiplier between the periodicity of the single-VENC functions if $VENC_H/VENC_L$ is a rational number. That was recently mathematically proven in a previous study.¹⁸ Therefore, unwrapping is produced when half-of the periodicity of J_{dual} is larger than the true velocity. This allows $VENC_H$ to be smaller than the true velocity, and it is not required to construct a third velocity with $iVENC$. The periodicity depends on β and it corresponds to $2aVENC_H$, $\beta = a/b$, with a, b positive integers. It can be verified that $iVENC$ match with $aVENC_H$ and $iVENC$ when $b = a + 1$.

It is important to mention that u^* results in a combined version of u_H and u_L . Therefore, its variance is not the same as the one of u_L . In case that u_H and u_L are independent identically distributed (i.i.d.), the variance is reduced as it was proven in a previous study.¹⁸ However, this is no longer the case when u_H and u_L share the background phase. In that case the variance of u^* maybe even larger than for u_L , depending on β . The detailed theoretical analysis is given in Appendix A.

In order to obtain comparable results with the other methods in terms of the variance of the unwrapped velocity, we will adopt a simpler (and also computationally cheaper) version of the ODV. To just use $J_{\text{dual}}(u)$ to guide the unwrapping of u_L , that is, to find u^* by solving,

$$k^* = \arg \min_{k \in \mathbb{Z}} J_{\text{dual}}(u_L + 2\text{VENC}_L k), \text{ subject to } -\text{VENC}_{\text{eff}} \leq u_L + 2\text{VENC}_L k \leq \text{VENC}_{\text{eff}} \quad (9)$$

where the effective VENC is $\text{VENC}_{\text{eff}} = \text{VENC}_H \frac{\beta}{1-\beta}$ and then to set $u^* = u_L + 2\text{VENC}_L k$. This leads to $\text{Var}(u^*) = \text{Var}(u_L) = 2\sigma_\varphi^2 \text{VENC}_L^2$, as in the other methods. This approach was introduced and applied to MR elastography recently.¹⁸

Optimal Dual-VENC Correction Algorithm

Here we propose a new approach to improve the results of the ODV method. In the presence of noise, all methods may fail to unwrap appropriately. However, in the case of the ODV, the cost function can be used to automatically detect potential failures and propose a corrected value.

To explain our ODV correction algorithm, an example is shown in the ascending aorta of a representative volunteer, Fig. 1a, with two pixels that the ODV method for $(\text{VENC}_H, \text{VENC}_L) = (75, 50)$ was not able to correct, restricted in the red rectangle. We analyzed four points in the region of interest (ROI), two of them still had aliasing (points 1 and 3), and the other pixels the ODV found the true velocity values (points 2 and 4) as shown in Fig. 1b. The presence of noise deforms the dual-VENC functions, as in Fig. 1c, then the global minima with the smallest absolute value will not be (close to) u_{true} , and velocity aliasing occurs, such as it occurs in points 1 and 3. Nevertheless, using the ODV formulation, we can correct it using the cost function values. Based on the considerations above, the ODV correction algorithm is as follows:

1. Locate 8-connected pixels for every image pixel for 2D.
2. Calculate the mean velocity of the neighborhood.
3. If this result does not have the same sign as the central pixel. Then, find the local minimum of $J_{\text{dual}}(u)$ with the smallest velocity value of the same sign as the neighborhood of the central pixel.
4. And finally, replace the velocity value corresponding to that local minimum of $J_{\text{dual}}(u)$ in the pixel of interest. The final result can be found in the Fig. 1d.

Methods

In Vivo Dataset

Two-dimensional PC-MRI data were acquired in 26 volunteers, age 32.4 ± 11.6 years (range 22–73 years, nine

females) using a clinical 1.5 T MR Scanner (Philips Achieva, Philips Medical Systems, Best, The Netherlands). The local committee approved the study, and informed consent was obtained from all participants. The protocol consisted of a through-plane 2D PC-MRI sequence perpendicular to ascending aorta above the Valsalva sinus. Acquisition parameters were: TE of 3.7 msec, TR of 5.5 msec, FA of 15° , VENCs of 50, 75, and 150 cm/second, field-of-view (FOV) of 320×116 mm, trigger time 27 msec, 25 cardiac phases using prospective ECG triggering, in-plane resolution $1 \times 1 \times 8$ mm,³ and temporal resolution between 35 and 48 msec. The raw data were obtained, and the reconstruction of each bipolar gradient was performed offline using MATLAB. Data from a five elements phased-array cardiac coil were combined using the method proposed by Bernstein et al.¹⁹ and Nett et al.²⁰ Since the acquisitions were performed using single-VENC protocols, we used the background phase from the scan with VENC_1 to reconstruct velocity image with the VENC_2 . To compare the methods, we only used representative peak-systolic phase, when more aliasing occurs.

The in vivo dataset was processed using an in-house MATLAB library (The MathWorks Inc., Natick, MA, USA), running in a 2.3 GHz Intel i7 processor equipped with 8 GB of RAM, which included the data reconstruction, the implementation of the unwrapping methods (SDV, ODV, and bi- and triconditional), the ODV correction algorithm, the addition of artificial noise, and the analysis of the results.

Additional (Synthetic) Noise

We simulated different levels of noise for the in vivo datasets. We assume three measurements with velocity encoding gradients $G_0 = 0 < G_H < G_L$, resulting in three measured complex magnetizations Z_{0k} , Z_{Hk} , and Z_{Lk} , for each coil $k = 1, \dots, 5$,

$$Z_{0k} = M_{0k} e^{i\theta_{0k}} \quad (10)$$

$$Z_{Hk} = M_{Hk} e^{i\theta_{Hk}}$$

$$Z_{Lk} = M_{Lk} e^{i\theta_{Lk}}$$

The modulus of Z_k provides the single-coil magnitude image, M_k , and the subscripts H and L are related to phases acquired with high- and low-VENCs, respectively, and 0 to the background phase. For all magnetization measurements, i.i.d. complex Gaussian noise $\varepsilon \tilde{\mathcal{N}}(0, \sigma^2)$ was added with a variance of $\sigma = M\{0, 5, 10, 15\}\%$, with M the maximal magnitude for all coils, voxels, and encoding gradients. Denoting the perturbed measurements with a “hat,” the phase-difference used in the velocity reconstruction for each voxel was computed by combining the measurements of the coils as

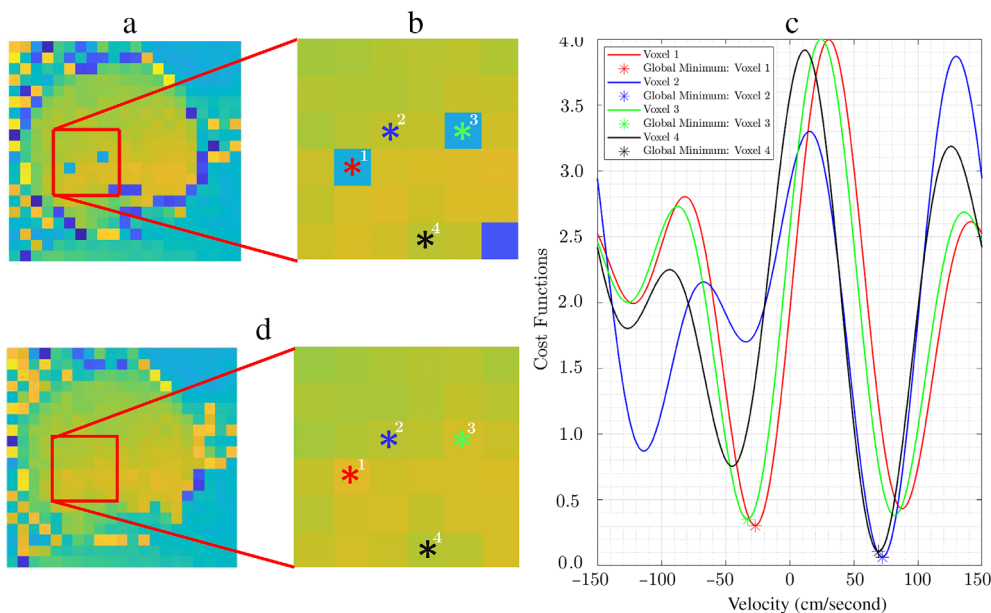


Figure 1: Two-dimensional PC-MRI for an ascending aorta of volunteer 1. (a) ODV 75, 50 marking ROI, red rectangle. (b) ROI's zoom with points of interest. (c) Cost functions vs. velocity for each point of interest, with the global minimum marked as asterisks. (d) Results of the ODV corrected methods marked the points of interest.

$$\Delta\Phi_{H,L} = \arg\left(\sum_k \widehat{Z}_{(H,L)k} \widehat{Z}_{0k}^*\right) \quad (11)$$

$$\Delta\Phi_i = \arg\left(\sum_k \widehat{Z}_{Hk} \widehat{Z}_{Lk}^*\right)$$

where $*$ denotes complex conjugate and $\arg(A + iB)$ is the angle between the positive real axis and the line joining 0 and $A + iB$, in radians. Finally, the velocities $u_{H,L,i}$ are given by,

$$u_{H,L} = \frac{\Delta\Phi_{H,L}}{\pi} \text{VENC}_{H,L} \quad (12)$$

$$u_i = \frac{\Delta\Phi_i}{\pi} i\text{VENC}$$

In order to compute the statistics of the results, we used 100 realizations of the noise.

VENC Combinations

In order to compare the methods, we used the following VENC combinations: $(\text{VENC}_H, \text{VENC}_L) = (150, 75)$ cm/second, $(\text{VENC}_H, \text{VENC}_L) = (150, 50)$ cm/second, and $(\text{VENC}_H, \text{VENC}_L) = (75, 50)$ cm/second, which resulted in $i\text{VENC}$ s of 150, 75, 150 cm/second, respectively. The reasoning is that, according to the theory, this provides an effective VENC values of 150 cm/second, respectively, for all methods, since $\beta = \text{VENC}_L/\text{VENC}_H = 1/2, 1/3,$ and $2/3$. Combining closer VENC values has been reported to have reduced noise robustness.¹⁸

Unwrapping Performance Quantification

To quantify and compare the performance of the methods, we counted the number of aliased of pixels after the unwrapping methods for each set of additional noise levels.

In order to analyze only the results within the aortic lumen, we applied binary masks. First, we converted the magnitude image into a binary image. Then, we calculated the distance transform for the binary image. Due to the fact that the ascending aorta (AAo) has a circular geometry, we used the watershed transform.²¹ Consequently, we identified the circle with the most extensive area. The segmentations were visually inspected and manually corrected if needed. Finally, we cropped the circles and automatically created the binary masks.

Then, we applied the same mask to the result of each unwrapping method and VENCs combination and counted the pixels whose sign differed from the $i\text{VENC}$ data.

Ethics Committee Approval

All subjects participated under informed consent, with data collection approved by the Ethical Committee of the Medical School at the Pontificia Universidad Católica de Chile and volunteers gave written informed consent for using their clinical data for research purposes.

Statistical Analysis

The datasets were checked for normality using a Shapiro-Wilk's normality test. The two-way analysis of variance was conducted to examine the unwrap pixels by using the unwrapping methods with different noise levels.

Homogeneity of variances was performed using Levene’s test, with a P -value <0.05 indicating statistical significance. Tukey’s multiple post hoc analysis with Bonferroni correction was performed for pair-wise comparison of unwrapping methods and two groups of noise levels. The results of the in vivo datasets were displayed in box-whisker plots. The statistical analysis was performed using the software R 4.1.1 (R Foundation for Statistical Computing, Vienna, Austria).²²

Results

Figure 2 illustrates the comparison of the unwrapping methods with different noise levels (0% and 10%) and VENCs combinations of a particular volunteer (26 years old, male). Figure S1 in the Supplemental Material shows the results for the same volunteer with 5% and 15% noise level. These examples demonstrated that without synthetic noise, all the methods delivered similar results. As expected, increasing the noise made all unwrapping methods less robust,

making the difference in the results of the methods more appreciable. Moreover, the figure shows the pixels where there was a difference between the ODV and the ODV corrected method (eighth column). It is important to mention that with $\beta = 1/2$, the number of pixels corrected was less than $\beta = 1/3$ and $\beta = 2/3$.

To quantify the performance of the methods, the results in terms of unwrapping success in the AAo of all volunteers with a different VENCs combination are shown in Fig. 3 and Fig. S2 in the Supplemental Material. Statistical analysis revealed that there were no extreme outliers, residuals were normally distributed ($P > 0.05$), and there was homogeneity of variances ($P > 0.05$). On the other hand, there was a statistically significant interaction between noise levels and the unwrapping method for the different VENCs combinations (i VENC, VENC_H, VENC_L) = (150, 150, 75), (i VENC, VENC_H, VENC_L) = (75, 150, 50), (i VENC, VENC_H, VENC_L) = (150, 75, 50). Consequently, we found which pairs of unwrapping methods differed using the Turkey test

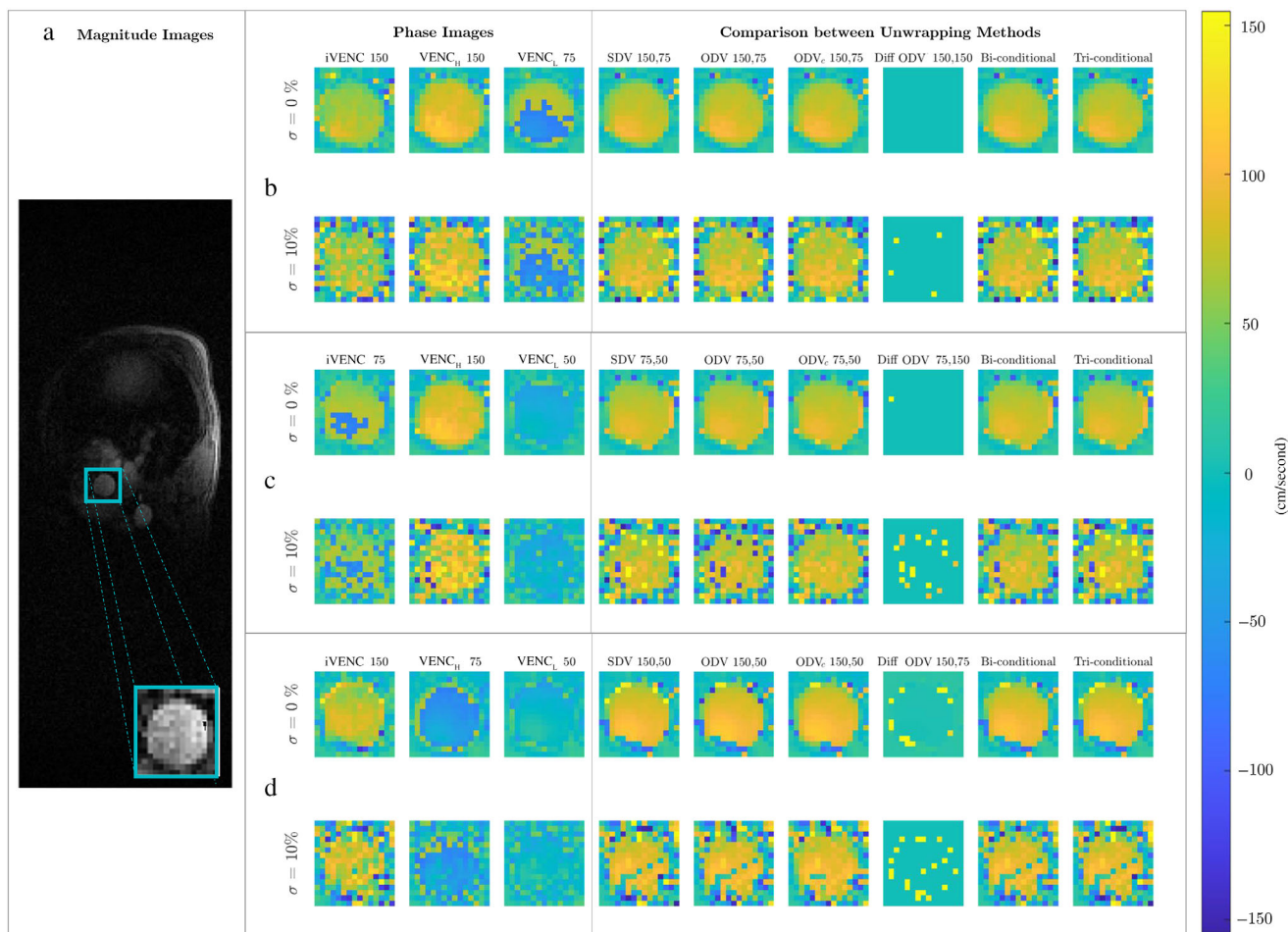


Figure 2: Ascending aorta at peak systole of a representative volunteer. (a) Magnitude images: slice prescription and region of interest. Phase-differences images with VENCs combination of (b) (i VENC, VENC_H, VENC_L) = (150, 150, 75), (c) (i VENC, VENC_H, VENC_L) = (75, 150, 50) cm/second and (d) (i VENC, VENC_H, VENC_L) = (150, 75, 50) cm/second with different levels of synthetic noise, σ . The VENCs used by the SDV and ODV methods are in the top part of the figures. First column: i VENC; second column: VENC_H; third column: VENC_L; fourth column: SDV; fifth column: ODV; sixth column: ODV corrected; seventh column: difference between the ODV and ODC corrected method; eighth column: biconditional; and ninth column: triconditional methods.

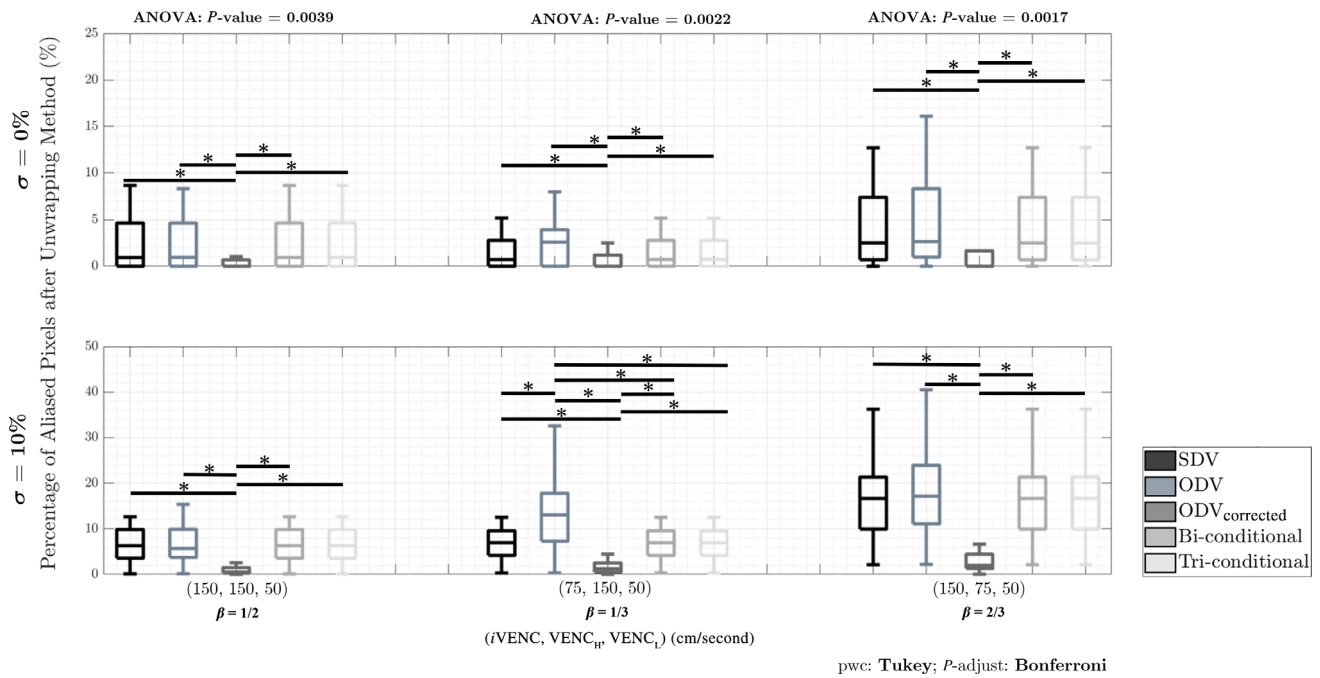


Figure 3: Box whisker plots for the evaluation of unwrapping methods of the volunteers at peak-systole in the ascending aorta with different levels of synthetic noise, σ , with VENCs combination of (first column) (iVENC, VENC_H, VENC_L) = (150, 150, 75) cm/second, (second column) (iVENC, VENC_H, VENC_L) = (75, 150, 50) cm/second, and (third column) (iVENC, VENC_H, VENC_L) = (150, 75, 50) cm/second. The SDV and ODV methods used in first column (VENC_H, VENC_L) = (150, 75) cm/second $\beta = 1/2$, second column (VENC_H, VENC_L) = (150, 50) cm/second $\beta = 1/3$, and third column, the SDV (iVENC, VENC_L) = (150, 50) cm/second $\beta = 1/3$, and the ODV method (VENC_H, VENC_L) = (75, 50) cm/second $\beta = 2/3$. Aliased number of pixels after the unwrapping methods were performed as a percentage. On each box, the central mark is the median, the bottom and top edges of the box are the 25th and 75th percentiles, respectively, and the whiskers extend to the most extreme data points not considered outliers. The significance of the interaction between noise levels and the unwrapping method for the different VENCs combinations is in the top part of the figures with their P -values. The symbol * indicates statistically significant differences ($P < 0.05$).

receiving a Bonferroni adjustment, indicated with the line mark and asterisk. These results revealed a significant difference between the ODV corrected and the other methods for $\beta = 1/2$, $\beta = 1/3$, and $\beta = 2/3$ for both noise levels analyzed ($\sigma = 0, 10\%$). Also, the ODV method presented statistically significant differences from the other methods with $\beta = 1/3$ and a noise level of 10%. Moreover, the figure shows the pixels where there was a difference between the ODV and the ODV corrected method (eighth column). It is important to mention that with $\beta = 1/2$, the number of pixels corrected were fewer than with $\beta = 1/3$ and $\beta = 2/3$.

For all methods and noise levels, the most robust VENC combination appeared to be $\beta = 1/2$, where VENC_H = VENC_{eff} and VENC_L = VENC_{eff}/2, for example, (VENC_H, VENC_L) = (150, 75) cm/second for (iVENC, VENC_H, VENC_L) = (150, 150, 75) cm/second. For $\beta = 1/3$, the reconstruction became less robust when increasing the noise level where VENC_H = VENC_{eff} and VENC_L = VENC_{eff}/3, for example, (VENC_H, VENC_L) = (150, 50) cm/second for (iVENC, VENC_H, VENC_L) = (75, 150, 50) cm/second. And finally, we obtained the less robust results with $\beta = 2/3$ where VENC_H = VENC_{eff}/2 and VENC_L = VENC_{eff}/3, for example, (VENC_H, VENC_L) = (75, 50) cm/second for (iVENC,

VENC_H, VENC_L) = (150, 75, 50) cm/second. Eventually, if β increased the distance in the cost functional is much smaller, which explained the errors of the method with $\beta = \{1/3, 2/3\}$, see details in.¹⁷

When comparing all methods, for each combination and noise level, the original ODV method showed the largest percentage of aliased pixels compared to the other of the methods for all VENC combinations and added noise. After that, the SDV, biconditional, and triconditional showed similar results. The best-performing method was the corrected ODV.

Computation times for a single volunteer dataset analyzed, the ODV and ODV_{corrected} were slower than the bi- and tri-conditional, and the SDV (ODV: ≈ 1.11 seconds, ODV_{corrected}: ≈ 1.242 seconds, biconditional: ≈ 0.007 seconds, tri-conditional: ≈ 0.008 seconds, and SDV: ≈ 0.003 seconds).

Discussion

This work reviewed, theoretically analyzed, and compared five unwrapping methods based on an in vivo dataset based on two acquired VENCs: the SDV, ODV, ODV corrected, and bi- and triconditional methods, where we developed the

ODV corrected method based on theoretical considerations. This is the first reported comparison of all these methods.

It was shown that the most robust unwrapping method appeared to be the corrected ODV method without noise. In contrast, the other methods showed similar performance in unwrapping success for all values of β tested in this work.

With the addition of synthetic noise to the in vivo datasets, the percentage of failed unwrapping increased for all values of β . We found that for $\beta = \text{VENC}_L / \text{VENC}_H = 1/2$ all methods performed similarly. These results were consistent with Carrillo et al.¹⁷ and Herthum et al.¹⁸ For that β value, the most robust unwrapping methods appeared to be the corrected ODV method ($P < 0.005$), obtaining the lowest failure percentage (mean values for: $\beta = 1/2$, 0.68% and 0.93% for noise levels of 0% and 10%, respectively; $\beta = 1/3$, 0.99% and 1.83% for noise levels of 0% and 10%, respectively; and $\beta = 2/3$, 3.94% and 4.36% for noise levels of 0% and 10%, respectively) compared with the other methods. Our statistical analysis can adequately determine the difference between the pair of unwrapping methods. We considered the mean percentage of aliased pixels after two unwrapping methods of 10% and 11%, respectively, and a standard deviation of 1% with a power of 0.8. Furthermore, the unwrapping method had similar behavior independent of the noise level. As expected, as noise level increased of the number of aliased pixels increases as well.

To make a fair comparison among all methods, we took full advantage of the VENCs proposed by Ma et al.¹⁶ For the SDV approach, in case $i\text{VENC} > \text{VENC}_H$, we used u_i rather than u_H as the original SDV would have used it, maintaining the effective VENC value. Otherwise, Lee et al.¹⁴ reported that the SDV method cannot handle the aliasing when both VENC values are lower than the maximum velocity.

Carrillo et al did not perform a detailed analysis of robustness of unwrapping methods to noise, only qualitatively on synthetic data. Here, we presented such analysis both numerically and theoretically. For the ODV method, here we used the “reduced” version recently reported by Herthum et al.¹⁸ This is based on the statistical analysis in Appendix A, which includes the fact that the velocity images shared the background phase with different VENC values. Furthermore, we developed a correction method for the ODV based on the additional information provided by the method. Although it works for single isolated pixels with incorrect values, it is important to mention that our algorithm may fail in a region with contiguous and wrapped pixels if the number of aliased pixels is similar to the number of pixels in the window kernel. Nevertheless, as we observed in the experiments, the correction algorithm worked adequately, even in extreme cases as when we added 15% noise to the images. In that case, we had a few contiguous pixels aliased, and the algorithm unwrapped most of them. Also, our correction required more

computational time than the ODV method. However, the ODV method was slower than SDV, bi-, and triconditional methods. Nevertheless, the computing time remained in the order of seconds, and therefore, it should not affect the applicability of the (corrected) ODV methods in clinical practice. It is important to clarify that we limited our study to methods where the velocity encoding is varied within the same spatial direction. Approaches using “diagonal” directions such as Johnson et al and Zwart and Pipe^{23,24} were not included in the analysis since they dealt with different input images.

Limitations

From the acquisition point of view, the PC-MRI data were acquired using standard single-VENC PC-MRI sequences. Nevertheless, we performed the acquisitions so that all other acquisition parameters except VENC had the same value. Further, we only used one common phase to process all data for all methods, and therefore, this single VENC acquisition would not affect the comparison of all methods. Another limitation is that all methods were assessed in healthy volunteers; future studies will investigate all methods in patients with stenotic valves, areas with high velocity, or in 4D-flow sequences of a large FOV. Another issue is that phase errors could arise from a patient’s motion during the MRI acquisition.²⁵ We attempted to control this factor to the best of our ability, as the acquisition was performed under breath-holds; any residual motion may have affected all methods similarly as all methods were acquired in the same scan session. Finally, although we tested the method on 26 volunteers, future work will use a flow phantom to test these methods in a controlled experiment. Using a phantom flow will allow us to test the Dual-VENC unwrapping methods under different conditions of flow (turbulent and retrograde conditions), noise, and resolutions.²⁶

Conclusions

In this study, we found that the quality of the results depends on the proportion of the VENCs of the input images, with $\text{VENC}_L / \text{VENC}_H = 0.5$ being the best performing combination for all methods. For that VENC combination, the most robust unwrapping method to noise was the corrected ODV approach, while the other methods showed similar performance in terms of unwrapping success.

Acknowledgments

The authors thank the Biomedical Imaging Center at Pontificia Universidad Católica de Chile for their support. This work has been funded by projects PIA-ACT192064, the Millennium Nucleus on Cardiovascular Magnetic Resonance NCN17_129, and ICN2021_004 of the Millennium Science Initiative Program of the National Agency for Research and

Development, ANID, as well as by the National Heart, Lung and Blood Institute grant F30HL137279. The authors also thank Fondecyt project 1181057 also by ANID. P. Franco thanks ANID—PCHA/Doctorado-Nacional/2018-21180391. H. Carrillo thanks CMM ANID PIA AFB170001 and project CORFO 10CEII-9157 Inria Chile.

Author Contributions

All authors were actively involved in reviewing and drafting the manuscript. All authors have approved the final version of this manuscript. Mainly, P.F. implemented the unwrapping methods, processed the MRI dataset, performed the noise analysis, developed the ODV correction method, participated in the study's design to recruit volunteers, and wrote the manuscript. L.M. and S.S. developed the bi- and triconditional unwrapping methods and edited the manuscript. H.C. participated in the noise analysis and edited the manuscript. C.M. acquired the in vivo MRI and edited the manuscript. M.M. participated in the study's design and edited the manuscript. C.B. co-developed the ODV method, participated in the study's design to recruit volunteers, participated in the mathematical noise analysis, in the study's design and empirical noise analysis, and edited the manuscript. S.U. participated in the study's design and edited the manuscript.

Conflict of Interest

The authors declare that they have no conflict of interest.

Data Availability Statement

The datasets generated during and/or analyzed during the current study are not publicly available due to data privacy according to the rules of Pontificia Universidad Católica de Chile but could be available from Sergio Uribe (suribe@uc.cl).

REFERENCES

- Markl M, Frydrychowicz A, Kozerke S, Hope M, Wieben O. 4D flow MRI. *J Magn Reson Imaging* 2012;36(5):1015-1036.
- Wu SP, Ringgaard S, Pedersen EM. Three-dimensional phase contrast velocity mapping acquisition improves wall shear stress estimation in vivo. *Magn Reson Imaging* 2004;22(3):345-351.
- Wigstrom L, Ebberts T, Fryrenius A, et al. Particle trace visualization of intracardiac flow using time-resolved 3D phase contrast MRI. *Magn Reson Med* 1999;41(4):793-799.
- Markl M, Harloff A, Bley TA, et al. Time-resolved 3D MR velocity mapping at 3T: Improved navigator-gated assessment of vascular anatomy and blood flow. *J Magn Reson Imaging* 2007;25(4):824-831.
- Kvitting JP, Ebberts T, Wigstrom L, Engvall J, Olin CL, Bolger AF. Flow patterns in the aortic root and the aorta studied with time-resolved, 3-dimensional, phase-contrast magnetic resonance imaging: Implications for aortic valve-sparing surgery. *J Thorac Cardiovasc Surg* 2004; 127(6):1602-1607.
- Stalder AF, Russe MF, Frydrychowicz A, Bock J, Henning J, Markl M. Quantitative 2D and 3D phase contrast MRI: Optimized analysis of blood flow and vessel wall parameters. *Magn Reson Med* 2008;60(5): 1218-1231.
- Markl M, Kilner PJ, Ebberts T. Comprehensive 4D velocity mapping of the heart and great vessels by cardiovascular magnetic resonance. *J Cardiovasc Magn Reson* 2011;13(1):7.
- Uribe S, Beerbaum P, Sørensen TS, Rasmusson A, Razavi R, Schaeffter T. Four-dimensional (4D) flow of the whole heart and great vessels using real-time respiratory self-gating. *Magn Reson Med* 2009; 62(4):984-992.
- Stadler A, Schima W, Ba-Ssalamah A, Kettenbach J, Eisenhuber E. Artifacts in body MR imaging: Their appearance and how to eliminate them. *Eur Radiol* 2007;17:1242-1255.
- Ha H, Kim GB, Kweon J, et al. Hemodynamic measurement using four-dimensional phase-contrast MRI: Quantification of hemodynamic parameters and clinical applications. *Korean J Radiol* 2016;17(4): 445-462.
- Pelc NJ, Bernstein MA, Shimakawa A, Glover GH. Encoding strategies for three-direction phase-contrast MR imaging of flow, journal of magnetic resonance imaging. *J Magn Reson Imaging* 1991;1(4):405-413.
- Yang GZ, Burger P, Kilner PJ, Karatowski SP, Firmin DN. Dynamic range extension of cine velocity measurements using motion-registered spatiotemporal phase unwrapping. *J Magn Reson Imaging* 1996;6(3): 495-502.
- Ghiglia D, Pritt MD. *Two-Dimensional Phase Unwrapping: Theory, Algorithms, and Software*. New York, USA: Wiley; 1998.
- Lee AT, Pike B, Pelc NJ. Three-point phase-contrast velocity measurements with increased velocity-to-noise ratio. *Magn Reson Med* 1995; 33(1):122-126.
- Schnell S, Ansari SA, Wu C, et al. Accelerated dual-VENC 4D flow MRI for neurovascular applications. *J Magn Reson Imaging* 2017;46(1): 102-114.
- Ma LE, Markl M, Chow K, Vali A, Wu C, Schnell S. Efficient triple-VENC phase-contrast MRI for improved velocity dynamic range. *Magn Reson Med* 2020;83(2):505-520.
- Carrillo H, Osses A, Uribe S, Bertoglio C. Optimal dual-VENC (ODV) unwrapping in phase-contrast MRI. *IEEE Trans Med Imaging* 2019; 38(5):1263-1270.
- Herthum H, Carrillo H, Osses A, Uribe S, Sack I, Bertoglio C. Multiple motion encoding in phase-contrast MRI: A general theory and application to elastography imaging. *Med Image Anal* 2022;14(78):102416. <https://doi.org/10.1016/j.media.2022.102416>.
- Bernstein MA, Mladen G, Brosnan TJ, Pelc NJ. Reconstructions of phase contrast, phased array multicoil data. *Magn Reson Med* 1994; 32(3):330-334.
- Nett EJ, Johnson KM, Frydrychowicz A, et al. Four-dimensional phase contrast MRI with accelerated dual velocity encoding. *J Magn Reson Imaging* 2012;35(6):1462-1471.
- Preim B, Botha C. *Visual Computing for Medicine: Theory, Algorithms, and Applications. The Morgan Kaufmann Series in Computer Graphics*. 2nd. Massachusetts, USA: Morgan Kaufmann; 2013.
- R Core Team. *R: A Language and Environment for Statistical Computing*. Vienna: R Foundation for Statistical Computing; 2013. Available from: <http://www.R-project.org/>.
- Johnson M, Markl M. Improved SNR in phase contrast velocimetry with 5-point balanced flow encoding. *Magn Reson Med* 2010;63(2): 349-355.
- Zwart NR, Pipe JG. Multidirectional high-moment encoding in phase contrast MRI. *Magn Reson Med* 2013;69:1553-1564.
- Bernstein MA, Shimakawa A, Pelc N. Minimizing TE in moment-nulled or flow-encoded two- and three-dimensional gradient-echo imaging. *J Magn Reson Imaging* 1992;2(5):583-588. <https://doi.org/10.1002/jmri.1880020517>.
- Montalba C, Uribina J, Sotelo J, et al. Variability of 4D flow parameters when subjected to changes in MRI acquisition parameters using a realistic thoracic aortic phantom. *Magn Reson Med* 2018;79(4):1882-1892. <https://doi.org/10.1002/mrm.26834>.

APPENDIX

A.1. Variance Analysis of the ODV Method

In order to calculate the statistical properties of u^* in the ODV method, we first need to obtain a closed expression for (an approximation of) it. Indeed, since the global minimum is also a local minimum, we calculated u^* using the fact that the solution is a local minimum of the cost function. Namely, we search for $J'_{\text{dual}}(u^*) = 0$, with

$$\begin{aligned} J'_{\text{dual}}(u^*) &= -\frac{\pi}{\text{VENC}_H} \sin\left(\frac{\pi}{\text{VENC}_H}(u_H - u^*)\right) - \frac{\pi}{\text{VENC}_L} \sin\left(\frac{\pi}{\text{VENC}_L}(u_L - u^*)\right) \\ &= -\frac{\pi}{\text{VENC}_H} \sin\left(\frac{\pi}{\text{VENC}_H}(u_H - u^* + 2k_H \text{VENC}_H)\right) - \frac{\pi}{\text{VENC}_L} \sin\left(\frac{\pi}{\text{VENC}_L}(u_L - u^* + 2k_L \text{VENC}_L)\right) = 0 \end{aligned} \quad (\text{A1})$$

In consequence, we can approximate the sin-terms by its arguments leading to:

$$u^* \approx (\text{VENC}_H^{-2} + \text{VENC}_L^{-2})^{-1} (u_H \text{VENC}_H^{-2} + u_L \text{VENC}_L^{-2} + 2(k_H \text{VENC}_H^{-1} + k_L \text{VENC}_L^{-1})) \quad (\text{A2})$$

Note first that the phases φ_o , φ_H , and φ_L are statistically independent with an expected value of $E[\varphi_i] = E[\varphi_o] + \frac{\bar{u}_i}{d_i} \pi$, where $i = H, L$ are related to velocities acquired with high and low VENCs. As a consequence, u_H and u_L are statistically dependent because both VENC images share the background phase. Therefore, the variance of u^* (Equation A2) has the form,

$$\begin{aligned} \text{Var}(u^*) &= (\text{VENC}_H^{-2} + \text{VENC}_L^{-2})^{-2} \\ &\quad \left(\text{Var}(u_H) \text{VENC}_H^{-4} + \text{Var}(u_L) \text{VENC}_L^{-4} + 2 \text{VENC}_H^{-2} \text{VENC}_L^{-2} \text{Cov}(u_H, u_L) \right) \\ &= (\text{VENC}_H^{-2} + \text{VENC}_L^{-2})^{-2} \left(2\sigma_\varphi^2 \text{VENC}_H^{-2} + 2\sigma_\varphi^2 \text{VENC}_L^{-2} + 2 \text{VENC}_H^{-2} \text{VENC}_L^{-2} \text{Cov}(u_H, u_L) \right) \\ &= \left(\frac{\text{VENC}_H^2 \text{VENC}_L^2}{\text{VENC}_H^2 + \text{VENC}_L^2} \right)^2 \left(2\sigma_\varphi^2 \text{VENC}_H^{-2} + 2\sigma_\varphi^2 \text{VENC}_L^{-2} + 2 \text{VENC}_H^{-2} \text{VENC}_L^{-2} \text{Cov}(u_H, u_L) \right) \\ &= 2\sigma_\varphi^2 (\text{VENC}_H^{-2} + \text{VENC}_L^{-2}) \left(\frac{\text{VENC}_H^2 \text{VENC}_L^2}{\text{VENC}_H^2 + \text{VENC}_L^2} \right)^2 + 2 \text{VENC}_H^{-2} \text{VENC}_L^{-2} \\ &\quad \left(\frac{\text{VENC}_H^2 \text{VENC}_L^2}{\text{VENC}_H^2 + \text{VENC}_L^2} \right)^2 \text{Cov}(u_H, u_L) \\ &= 2\sigma_\varphi^2 \frac{\text{VENC}_H^2 \text{VENC}_L^2}{\text{VENC}_H^2 + \text{VENC}_L^2} + 2 \frac{\text{VENC}_H^2 \text{VENC}_L^2}{(\text{VENC}_H^2 + \text{VENC}_L^2)^2} \text{Cov}(u_H, u_L) \\ &= \frac{\text{Var}(u_H)}{1 + \beta^2} + \frac{2 \text{VENC}_H^2 \text{VENC}_L^2}{(\text{VENC}_H^2 + \text{VENC}_L^2)^2} \text{Cov}(u_H, u_L) \\ &= \frac{\text{Var}(u_H)}{1 + \beta^2} + \frac{2 \text{VENC}_H^2 \text{VENC}_L^2}{(\text{VENC}_H^2 + \text{VENC}_L^2)^2} E[(u_H - E u_H)(u_L - E u_L)] \\ &= \frac{\text{Var}(u_L)}{1 + \beta^2} + \frac{2 \text{VENC}_H^2 \text{VENC}_L^2}{(\text{VENC}_H^2 + \text{VENC}_L^2)^2} \left(E \left[\left(\frac{\varphi_H - \varphi_o}{\pi} \text{VENC}_H \right) \left(\frac{\varphi_L - \varphi_o}{\pi} \text{VENC}_L \right) \right] - \bar{u}_H \bar{u}_L \right) \\ &= \frac{\text{Var}(u_L)}{1 + \beta^2} + \frac{2 \text{VENC}_H^2 \text{VENC}_L^2}{(\text{VENC}_H^2 + \text{VENC}_L^2)^2} \left(\frac{\text{VENC}_H \text{VENC}_L}{\pi^2} (E[\varphi_o^2] - E[\varphi_o]^2) \right) \\ &= \frac{\text{Var}(u_L)}{1 + \beta^2} + \frac{2 \text{VENC}_H \text{VENC}_L}{(1 + \beta^2) \pi^2} \text{Var}(\varphi_o) \end{aligned}$$

$$= \frac{\text{Var}(u_L)}{1 + \beta^2} \left(1 + \frac{\beta}{(1 + \beta^2)} \right) \tag{A3}$$

For this calculation, we considered $\text{Var}(\varphi_0) = \pi^2 \sigma_\varphi^2$, $\text{Var}(u_L) = 2\sigma_\varphi^2 \text{VENC}_L^2$, and $\text{Var}(u_H) = 2\sigma_\varphi^2 \text{VENC}_H^2$. Note that the covariance is defined as the expected value of the product of their deviations from their individual expected values $\text{Cov}(u_H, u_L) = E[(u_H - E u_H)(u_L - E u_L)]$ and the expression for the variance, for example, for the φ_0 can be expanded as, $\text{Var}(\varphi_0) = E[(\varphi_0 - E[\varphi_0])^2] = E[\varphi_0^2 - 2\varphi_0 E[\varphi_0] + E[\varphi_0]^2] = E[\varphi_0^2] - 2E[\varphi_0]E[\varphi_0] + E[\varphi_0]^2 = E[\varphi_0^2] - E[\varphi_0]^2$.

Now we want to calculate the β values ($\text{VENC}_L = \beta \text{VENC}_H, 0 < \beta < 1$) such that the variance of the result with the ODV method is equal to or lower than the low VENC image, i.e., $\text{Var}(u^*) \leq \text{Var}(u_L)$,

$$\text{Var}(u^*) = \frac{\text{Var}(u_L)}{1 + \beta^2} \left(1 + \frac{\beta}{(1 + \beta^2)} \right) \leq \text{Var}(u_L) \tag{A4}$$

Equation A4 becomes

$$\beta^4 + \beta^2 - \beta \geq 0 \tag{A5}$$

We could find the solutions for Equation A5, factorizing by β and using the zero-factor theorem for $\beta \neq 0$,

$$\beta^3 + \beta - 1 \geq 0 \tag{A6}$$

Therefore, an improved estimate in terms of variance is obtained,

$$\frac{\text{Var}(u_L)}{1 + \beta^2} \left(1 + \frac{\beta}{(1 + \beta^2)} \right) \leq \text{Var}(u_H), \text{ if } \beta \geq 0.682 \tag{A7}$$